J Mater Sci: Mater Electron (2013) 24:916–926
DOI 10.1007/s10854-012-0850-2

Effect of divalent cation substitution in the magnetoplumbite structured $BaFe_{12}O_{19}$ system

Venugopalan Anbarasu · P. M. Md Gazzali · Thangavelu Karthik · Appasamy Manigandan · Kandasamy Sivakumar

Received: 21 June 2012 / Accepted: 23 July 2012 / Published online: 10 August 2012

Abstract Synthesis of magnetically ordered barium hexaferrite powders and the adjustment of magnetic properties for perpendicular magnetic recording media are realized through substitution of divalent cation (Ca) in the $BaFe_{12}O_{19}$ system. The Ca^{2+} substituted $Ba_{1-x}Ca_xFe_{12}O_{19}$ (where x = 0.05, 0.1, 0.15 and 0.2) compounds have been prepared through solid state reaction technique. The powder X-ray diffraction analysis reveals that all the prepared compounds crystallized in magnetoplumbite hexagonal structure and the flat hexagonal platelet morphology of the crystallites was identified through scanning electron microscopy. The formation of magnetoplumbite structured $Ba_{1-x}Ca_xFe_{12}O_{19}$ system due to mechanical activation was supported by micro-Raman measurements. Both pure and Ca substituted $BaFe_{12}O_{19}$ compounds exhibit sharp intense peaks which reveals defect free environment in the crystal lattice. From the room temperature magnetization studies, it was observed that the saturation magnetization (M_S) and remanent magnetization (M_R) values drastically decreases for the $Ba_{0.95}Ca_{0.05}Fe_{12}O_{19}$ compound which may be due to the existence of spin canting effect and leads to the reduction of super exchange fields. The increase in M_S and M_R values for the $Ba_{0.9}Ca_{0.1}Fe_{12}O_{19}$ and $Ba_{0.85}Ca_{0.15}Fe_{12}O_{19}$ compounds could be attributed to the enhanced hyperfine fields at 12k and 2b sites due to the strengthening of Fe^{3+}–O–Fe^{3+} super exchange interactions. A large reduction in the coercivity value from 3,090 to 1,548 Gauss may be attributed to the fall in magneto crystalline anisotropy. The high temperature magnetization studies infer that while increasing substitution level of Ca in the $BaFe_{12}O_{19}$ system results in decreasing trend in Curie temperature. The room temperature dielectric measurement shows that the incorporation of Ca^{2+} in the $BaFe_{12}O_{19}$ system results with increase in the dielectric constant and this case substantiates the space charge polarization. The magnetically ordered BaFe particulate having higher saturation and low coercivity values with superior magnetic and dielectric behaviour exhibiting the possibility for future high-recording-density storage products.

V. Anbarasu (✉)
Department of Physics, SRM University, Ramapuram Campus, Chennai 600089, India
e-mail: anbarasu100@gmail.com

P. M. Md Gazzali
Department of Physics, Pondicherry University, Kalapet 605014, Pudhucherry, India

T. Karthik
Department of Materials Science and Engineering, Indian Institute of Technology Hyderabad, Yeddumailaram 502205, India

A. Manigandan
Department of Physics, University College of Engineering, Kanchipuram 631552, India

K. Sivakumar
Department of Physics, Anna University, Chennai 600025, India

1 Introduction

Magnetic ceramics have found commercial applications ever since 1940s. A wide range of substitutional solid solubility makes it possible to "tailor" the magnetic properties of polycrystalline magnetic ceramics over a range of curie points, remanent magnetization, saturation magnetization and coercive fields. Thus, ceramic magnets can be molecularly designed and processed for specific electronic applications, such as audio and video recording tapes, microwave absorbers, motors, generators and

computer disks. Magnetic ceramics are well known for their high resistivity, low eddy current loss at higher frequencies and also low cost, which makes it beneficial than their metal and metal alloys counterpart [1].

Barium ferrites are well known hard magnetic materials, which are based on iron oxide. They are also called as ferrite magnets and could not be easily replaced by any other magnets [2]. Barium hexaferrite ($BaFe_{12}O_{19}$) is the model for a family of 'M-type ferrites' because of they are based upon the hexagonal magnetoplumbite structure. Its crystal structure related to that of the spinels and having much more complex. The large unit cell (a = 5.88 Å; c = 23.2 Å) contains two formula units, i.e. a total of 64 ions. The Ba^{2+} and O^{2-} ions together form a close-packed structure with some of the layers cubic close-packed and others hexagonal close-packed [3]. Its symmetry is characterized by the space group $P6_3/mmc$.

The structure of $BaFe_{12}O_{19}$ is built up from a cubic block 'S' having the spinel structure and a hexagonal block 'R' containing the Ba-ions. Five oxygen layers make one molecule and two molecules make one unit cell. In the unit cell, Fe^{3+} ions occupy five different crystallographic sites, i.e., tetrahedral ($4f_1$), octahedral (12k, 2a, $4f_2$) and hexahedral (2b) site of oxygen lattice. In the magnetically ordered state of $BaFe_{12}O_{19}$, the 12k, 2a, and 2b sites have their spins parallel to the crystallographic c-axis, whereas those of $4f_1$ and $4f_2$ points are anti-parallel, constituting a net magnetic moment of 40 μB [4, 5]. In addition, $BaFe_{12}O_{19}$ possesses a unique combination of desirable properties such as low production cost, high saturation magnetization (Ms = 72 emu/g), high coercive force (H_C = 6,700 Oe), high Curie temperature (720 K), magneto crystalline anisotropy along c-axis (Ha = 1.7 T), chemically stable and corrosion resistant. Due to these properties, it has a wide range of applications in the high-performance permanent magnetic material, magnetic recording media, ferrofluids, sensors, microwave absorbtion, loud speakers and the rotors in small DC motors [6].

To tailor the magnetic properties of the barium hexaferrites, Fe^{3+} ions are partially substituted by various di, tri, and tetravalent ions, aiming to occupy the spin down sites and consequently to increase the net magnetization. It has been also predicted that properties such as thermal and electrical conductivity, magnetic, electrical and optical behavior could be enhanced in materials by substitution with rare earth elements. Nevertheless, if Fe^{3+} is substituted by a divalent ion, a simultaneous substitution (e.g., of a Ba^{2+} by a trivalent ion) is necessary to satisfy the condition of charge balance [7–9]. Actually, a simple partial Ba^{2+} substitution by a trivalent rare earth ion (e.g., La^{3+}, Nd^{3+}, Sm^{3+}) induces the valence change of Fe^{3+} to Fe^{2+} and depending on the substitutional rare earth ion, enhance the magnetization and/or coercivity [10, 11]. Besides that, the simultaneous substitution of divalent–tetravalent ions for Fe^{3+} is another approach which satisfies the electronic neutrality criteria [4]. Recently, the interest in the studies of structural and magnetic properties of M-type $BaFe_{12}O_{19}$ compound by substituting di and tri valent elements has increased drastically. The reports suggest that the substitution of other elements at Ba and/or Fe site has strong influence on both structural and magnetic properties [12–14].

Many researchers have emphasized the modification of magnetic properties of $BaFe_{12}O_{19}$ compound by the substitution of Fe^{3+} with other ions such as Co^{2+}, Ti^{4+}, Ni^{2+}, Sn^{4+}, Cr^{3+} and Al^{3+}. The early researches indicated that the La^{3+} ions can be totally substituted into the site of Ba^{2+} ions, suggesting change in Fe^{3+} ions to Fe^{2+} ions on 2a crystallographic sites [15, 16]. Recently, Javed Iqbal et al. [17] reported calcium substituted $Sr_{1-x}Ca_xFe_{12}O_{19}$ nano hexaferrites prepared through co-precipitation technique. From the powder XRD analysis, it was reported that the material has a single magnetoplumbite phase containing calcium content in the range 0.0–0.2. An increase in the stoichiometric amount of calcium results in a nonmagnetic α-Fe_2O_3 phase as an impurity along with the magnetoplumbite phase while calcined at 920 °C for 1 h. The variations of dielectric constant and dielectric loss angle were explained on the basis of Maxwell–Wagner and Koops models and it was finalized that the enhanced resistivity of the calcium doped material has potential applications in microwave devices.

Further, Ashima et al. reported the synthesis and characterization of $Ba_{0.5}Ca_{0.5}Fe_{12}O_{19}$ compound prepared by solid state reaction method. They reported that the substitution of Ca in Ba site of $BaFe_{12}O_{19}$ system leads to compactness in the magnetoplumbite based crystal structure, reduction in saturation magnetization from 53.03 to 33.17 emu/g and increasing the resistivity, which results in decreasing trend in the dielectric loss factor [18].

In the literature, much report are available on the combinational substitution of di, tri and tetravalent ions in Ba and Fe site of $BaFe_{12}O_{19}$, whereas the systematic substitution of Ca on the Ba site of $BaFe_{12}O_{19}$ compound is not yet reported. Hence in the present work, substitution of divalent, non-magnetic calcium ion (Ca^{2+}) in the Ba^{2+} site of $BaFe_{12}O_{19}$ system has been carried out to estimate the possible changes in its magnetic properties.

The ceramic compounds $Ba_{1-x}Ca_xFe_{12}O_{19}$ (where x = 0, 0.05, 0.1, 0.15 and 0.2) were prepared through solid state reaction technique by subsequent annealing. Powder X-ray diffraction, scanning electron microscopy, EDX analysis, micro Raman spectroscopy, room temperature and high temperature magnetization measurements and dielectric measurements were carried out for their characterization. The results observed from the above mentioned studies are briefly discussed below.

2 Experimental

Ceramics of solid solution $Ba_{1-x}Ca_xFe_{12}O_{19}$ was prepared through conventional mixed–oxide technique at a temperature of 1,110 °C. Barium Carbonate ($BaCO_3$ ~ 99.99 % purity), Calcium Carbonate ($CaCO_3$ ~ 99.99 % purity) and Iron Oxide (Fe_2O_3 ~ 99.99 % purity) were carefully weighed in stoichiometric proportions and thoroughly mixed in an agate mortar for about 1 h using high purity acetone as a medium. The sample was calcined at 900 °C for 24 h in an alumina crucible. The calcined material was once again ground thoroughly prior to intermediate sintering at 1,000 °C and 1,100 °C for 24 h. Then the samples were reground and pelletized for the final annealing process. The pelletized samples were finally annealed at 1,110 °C for 24 h and to obtain homogeneity, slow cooling process was adopted at a rate of 5 °C/h up to 500 °C in the air atmosphere. The hard sintered samples obtained from final annealing process were utilized for further characterization studies.

The structure identification of the compounds was carried out using a Rigaku Ultima III X-ray Diffractormeter with CuKα1 radiation ($\lambda = 1.5406$ Å). The microstructure and elemental compositions of the samples were studied simultaneously using Quanta 200 FEG high resolution scanning electron microscope which has the analytical capability of detecting elements with help of energy dispersive X-ray spectrometry. Polarized Raman spectra of the polycrystalline samples were recorded with a dispersive micro Raman spectrometer equipped with a microscope (Bruker SENTERRA). The room temperature and high temperature magnetization nature of the prepared compounds was analyzed through LAKE SHORE (Model: 7404) vibrating sample magnetometer (VSM) and the dielectric measurements have been carried out with HIOKI 3532–50 LCR HITESTER.

3 Results and discussion

3.1 Powder X-ray diffraction analysis

The observed powder XRD patterns of the prepared powder samples $Ba_{1-x}Ca_xFe_{12}O_{19}$ (where x = 0–0.1) are shown in Fig. 1, which reveals the magnetoplumbite phase formation of all the compounds. It is also observed that substitution level of Ca in the $BaFe_{12}O_{19}$ system results with decrease in intensity of major diffraction peaks which confirms the incorporation of Ca into the lattice of $BaFe_{12}O_{19}$. The lattice parameters of pure and Ca substituted $BaFe_{12}O_{19}$ compounds have been calculated using PowderX, a program for powder X-ray diffraction data processing [19]. A comparative statement of lattice parameters observed for all the prepared compounds are listed in Table 1. The variation in lattice parameters with

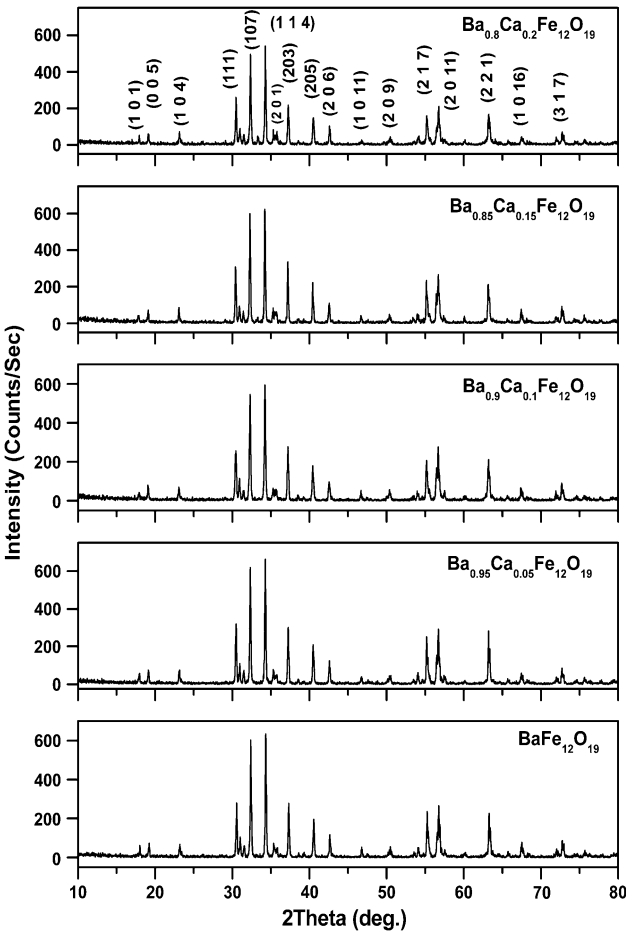

Fig. 1 Powder X-ray diffraction patterns of the $Ba_{1-x}Ca_xFe_{12}O_{19}$ compounds

respect to concentration of Ca in $Ba_{1-x}Ca_xFe_{12}O_{19}$ system is graphically shown in Fig. 2. It shows that both pure and calcium substituted $BaFe_{12}O_{19}$ compounds are in magnetoplumbite structure only. It is also observed that the value of the lattice constant 'a' remains almost same but the value of 'c' decreases with increase in the calcium content which may be due to smaller ionic radii element Ca^{2+} (0.99 Å) replacing Ba^{2+} (1.35 Å) site in $BaFe_{12}O_{19}$ system [17, 20].

Table 1 Comparative statement of lattice parameter observed for pure and Ca substituted $BaFe_{12}O_{19}$ compounds

Compound	a (Å)	c (Å)	Volume (Å^3)	System
$BaFe_{12}O_{19}$ (Ref) JCPDS: 84-0757	5.892	23.183	696.99	Hexagonal
$BaFe_{12}O_{19}$	5.890(3)	23.197(1)	696.98	Hexagonal
$Ba_{0.95}Ca_{0.05}Fe_{12}O_{19}$	5.892(2)	23.145(9)	696.09	Hexagonal
$Ba_{0.9}Ca_{0.1}Fe_{12}O_{19}$	5.891(3)	23.129(4)	695.22	Hexagonal
$Ba_{0.85}Ca_{0.05}Fe_{12}O_{19}$	5.887(1)	23.124(7)	694.19	Hexagonal
$Ba_{0.8}Ca_{0.2}Fe_{12}O_{19}$	5.889(2)	23.101(9)	694.05	Hexagonal

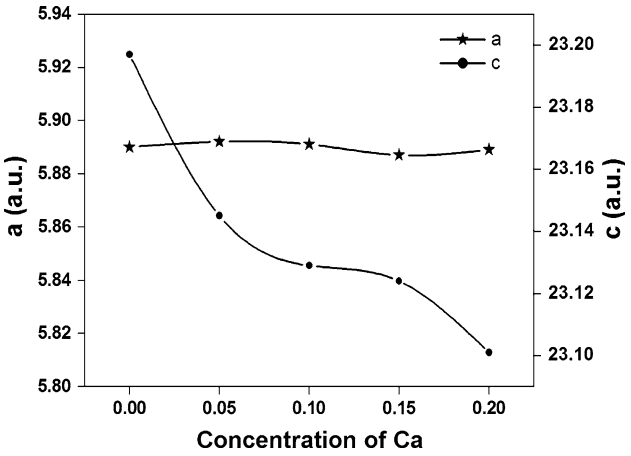

Fig. 2 Lattice parameters a and c of $Ba_{1-x}Ca_xFe_{12}O_{19}$ compounds as a function of x

3.2 Surface morphology and elemental analysis

In the present work, for the analysis of morphology and elemental composition, internal portion of pelletized samples annealed at 1,110 °C are used. The images observed from the internal portion of the pelletized samples are shown in Fig. 3 and it is observed that all the samples crystallize in micro range with well crystalline nature. The samples present a heterogeneous distribution of grains. The grains appear to stick each other and agglomerate in different masses throughout the micrograph. On higher magnification, it is identified that the morphology is much more uniform with flat hexagonal plates and this morphology is typical for phases having M-type ferrites [21]. There is clear evidence that some of these grains have coalesced to form larger grains within the material formed at high temperature as a consequence of thermodynamically driven mass diffusion mechanisms. It is also to be noted here that there are some pores present in the micro structure of pure and Ca substituted $BaFe_{12}O_{19}$ compounds and that is unavoidable since 100 % theoretical density is never achieved during any sintering process [16]. The EDX analysis confirms the composition of the $Ba_{1-x}Ca_xFe_{12}O_{19}$ (where x = 0.05, 0.1, 0.15 and 0.2) compounds. The increasing concentration of Ca while comparing with the parent compound was also identified through this analysis.

3.3 Micro-Raman analysis

Raman spectroscopy involves molecular and crystal lattice vibrations and is therefore sensitive to the composition, bonding, chemical environment, phase and crystalline structure of the sample material in any physical form. In the present work, Raman spectroscopy has been used to show the phase composition and homogeneity of the pure and Ca substituted $BaFe_{12}O_{19}$ system by comparing the observed results with the selection rules and mode assignments discussed by Kreisel et al. [22]. From the literature, it is reported that 42 Raman-active modes ($11A_{1g} + 14E_{1g} + 17E_{2g}$) and 30 IR active modes ($13A_{2u} + 17E_{1u}$) are expected for the barium hexaferrite system ($BaFe_{12}O_{19}$). Raman spectra of all the prepared compounds were recorded and normalised with respect to the most intense band at room temperature. In order to analyze the polarization dependence of the Raman signals, the Raman bands were fitted with the Lorentzian line shape and the results are shown in Fig. 4. The observed Raman spectra have been indexed and the comparative statement of vibrational modes observed was listed in the Table 2. A brief discussion about these results is given below.

- All the obtained Raman spectra show a marked polarization effect, which indicates a good orientation and a good crystalline quality of all the prepared compounds.
- The pure and Ca substituted $BaFe_{12}O_{19}$ compounds showing the sharp intense peaks which reveals defect free environment in the $Ba_{1-x}Ca_xFe_{12}O_3$ compounds and shows the high crystalline nature of the prepared compounds.
- The strong peaks observed at about 713, 686, 527, 467, 451, 420, 410, 385, 285, 212, 183 and 171 cm^{-1} are in good agreement with the magnetoplumbite structure.
- The incorporation of E_{2g} mode of vibration with corresponding resonance peaks at about 566 and 335 cm^{-1} confirms the effect of Ca substitution in divalent site.
- Upon increasing the concentration of calcium in $BaFe_{12}O_{19}$, the presence of a weak band at about 340 cm^{-1} may be assigned with A_{1g} or E_{1g} mode corresponds to mixed octahedra of M-type structures.
- It should be noted that none of the spectra show the expected number of bands. For the case of barium hexaferrite, at room temperature, the spectra of $BaFe_{12}O_{19}$ should exhibit 42 Raman active modes ($11A_{1g} + 14E_{1g} + 17E_{2g}$). The intensity of resonance signals of some of the bands is quite large which leads to overlapping, at least partially. The progressive broadening of the resonance bands of pure and Ca substituted $BaFe_{12}O_{19}$ compounds can be explained by a smaller domain size and a higher contribution of domain boundaries. It is also reported that the possibility of overlapping in resonance bands may due to local stress and a large number of point defects leading to a local lowering of symmetry [23].
- From the Raman spectroscopy analysis, it is confirmed that the pure and Ca substituted compounds belong to magnetoplumbite crystalline structure. The variation in resonance peak positions observed in the frequency

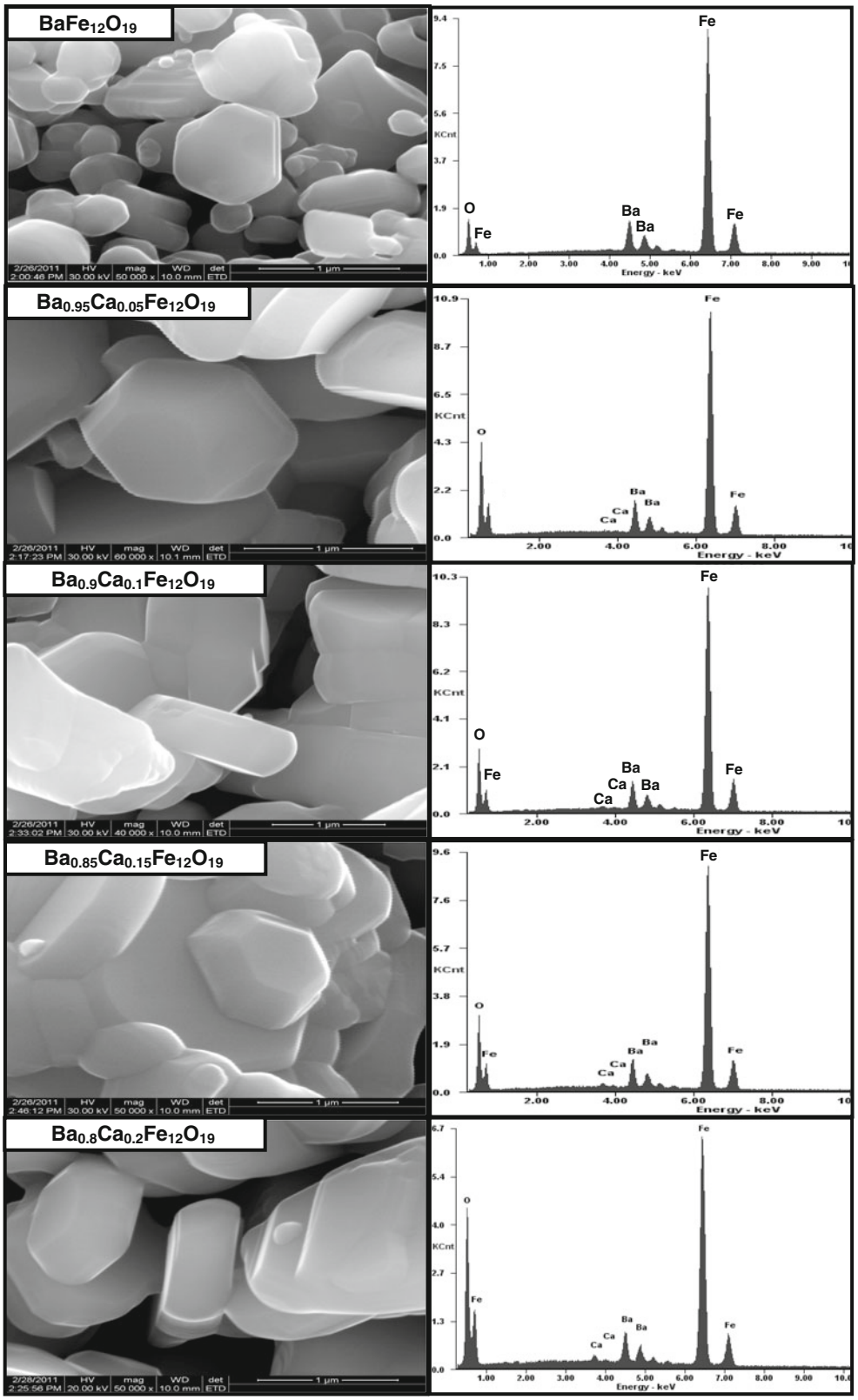

Fig. 3 Morphology and EDX spectrum of pure and Ca substituted $Ba_{1-x}Ca_xFe_{12}O_{19}$ compounds

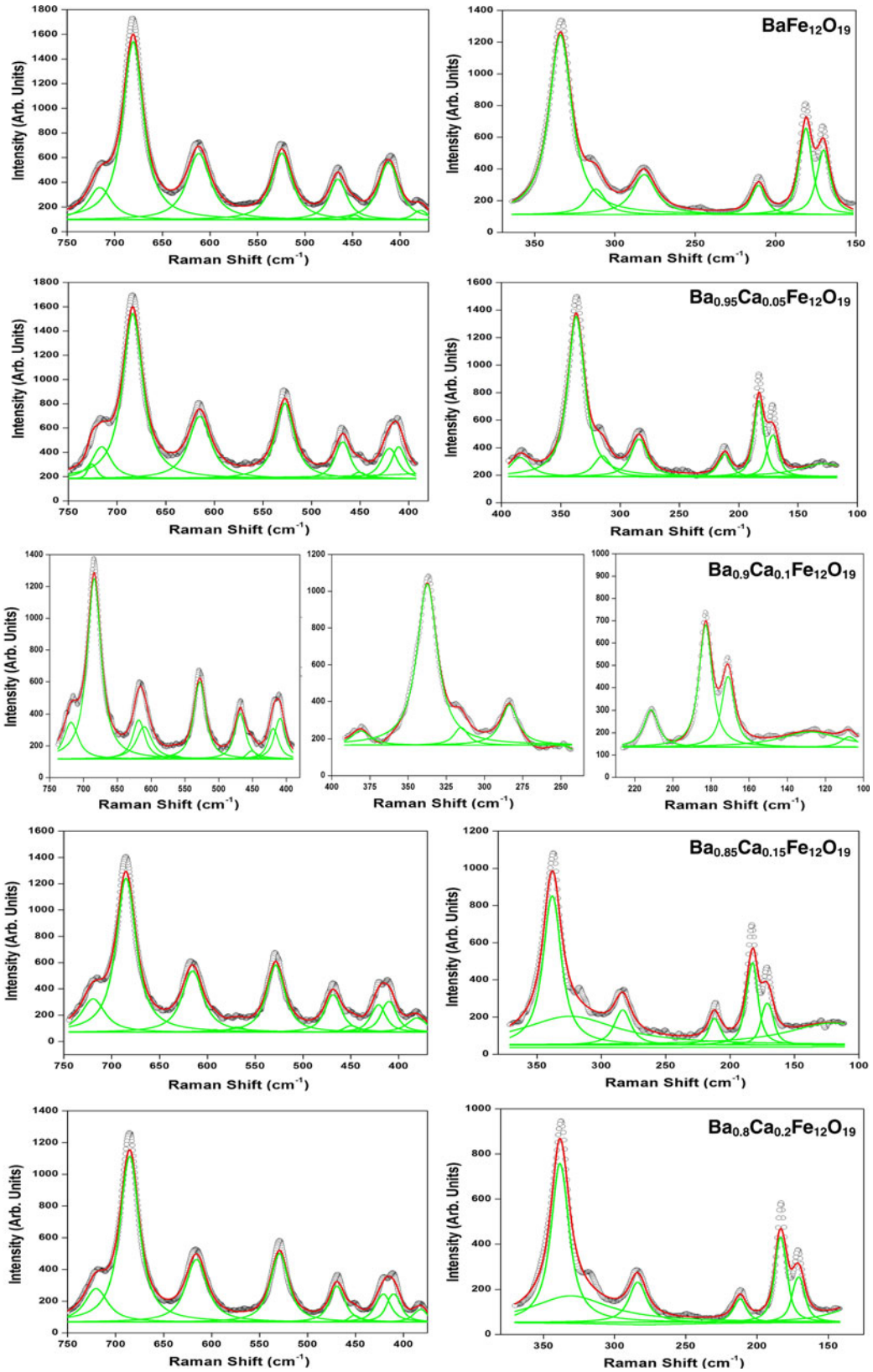

Fig. 4 Fitting curves of the Raman signal for the $Ba_{1-x}Ca_xFe_{12}O_{19}$ compounds with Lorentzian line shapes The *open circles* are experimental data, the *strong curves with green shade* are the fitting of Lorentzian shapes and the *solid curves with red shade* are the total intensities of the Lorentzian lines (Color figure online)

Table 2 Symmetry assignment for the Raman spectrum of $Ba_{1-x}Ca_xFe_{12}O_{19}$ compounds

Details of the compound					Ref.	Symmetry assignments	
Ba	$Ba_{0.95}$	$Ba_{0.9}$	$Ba_{0.85}$	$Ba_{0.8}$			
	725	718	719	720	722	A_{1g}	Tetrahedra $Fe^{(3)}O_4$
716	716				713	A_{1g}	Tetrahedra $Fe^{(3)}O_4$
681	684	684	685	686	684	A_{1g}	Bipyramid $Fe^{(2)}O_5$
	615	618	615	614	613	A_{1g}	Octahedra $Fe^{(4)}O_6$
		611			612	E_{1g}	Octahedra (mixed)
		565	569		566	E_{2g}	
524	527	528	528	527	527	E_{1g}	
		511			512	A_{1g}	Octahedra $Fe^{(1)}O_6$ and $Fe^{(5)}O_6$
465	468	467	469	467	467	A_{1g}	Octahedra $Fe^{(1)}O_6$ and $Fe^{(5)}O_6$
448	451	452	449	451	451	E_{1g}	
	420	419	421	420	420	E_{2g}	
412	410	410	410	410	409	A_{1g}	$Fe^{(5)}O_6$ octahedra dominated
379	384	381	381	382	385	E_{2g}	
			338	338	340	A_{1g}	Octahedra (mixed)
			338	338	340	E_{1g}	
334	337	337		331	335	E_{2g}	
312	315	315			317	A_{1g}	
282	284	285	283	284	285	E_{1g}	
211	212	211	212	212	212	E_{1g}	
181	183	184	183	183	184	E_{1g}	Whole spinel block
170	171	173	173	171	173	E_{1g}	Whole spinel block

range of below 150 cm^{-1} clearly shows the effect of substitution in divalent cation on the $BaFe_{12}O_{19}$ system.

3.4 Magnetization studies

3.4.1 Room temperature magnetization studies

The magnetic characteristics of $Ba_{1-x}Ca_xFe_{12}O_{19}$ (where x = 0, 0.05, 0.1, 0.15 and 0.2) compounds were recorded at room temperature using a VSM at a maximum field of 12,000 Gauss. The magnetic hysteresis loops observed for the $Ba_{1-x}Ca_xFe_{12}O_{19}$ compounds were shown in Fig. 5. The hysteresis behaviour implies high coercivity and non-saturation nature of the samples up to the field of 12,000 Gauss. It is reported that $BaFe_{12}O_{19}$ has a very high anisotropy field of 17,000 Gauss by which the prepared samples are not saturated at 12,000 Gauss [24]. The remanent magnetization (M_R), saturation magnetization (M_S) and coercive field (H_C) were determined from the M-H measurements and observed values are listed in Table 3. From the table, it is observed that the saturated magnetization value attained by the pure $BaFe_{12}O_{19}$ compound at 12,000 Gauss is 63.74 emu/g, which is in good agreement with the earlier reports [25, 26]. It is also observed that the M_S and M_R values drastically decreases for $Ba_{0.95}Ca_{0.05}Fe_{12}O_{19}$ compound and then increases for $Ba_{0.9}Ca_{0.1}Fe_{12}O_{19}$ and $Ba_{0.85}Ca_{0.15}Fe_{12}O_{19}$ compounds. However for the $Ba_{0.8}Ca_{0.2}Fe_{12}O_{19}$ compound, the saturation magnetization value again decreases. It is to be noted that the maximum saturation magnetization value achieved by the $Ba_{0.85}Ca_{0.15}Fe_{12}O_{19}$ compound (65.05 emu/g) is somewhat higher than the pure $BaFe_{12}O_{19}$ compound. The dependence of saturation magnetization with respect to coercive field is graphically given in Fig. 6.

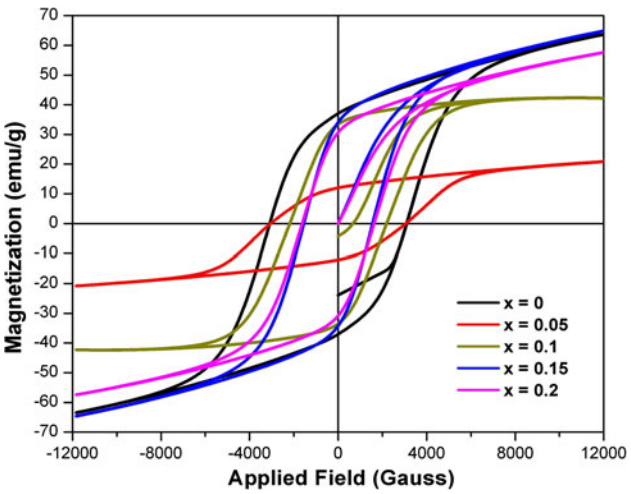

Fig. 5 Magnetization nature of $Ba_{1-x}Ca_xFe_{12}O_{19}$ compounds

Table 3 Magnetic parameters of the $Ba_{1-x}Ca_xFe_{12}O_{19}$ compounds

Sample details	M_S (emu/g)	M_R (emu/g)	H_C (Gauss)	Squareness ratio (M_R/M_S)
$BaFe_{12}O_{19}$	63.74	37.07	3090	0.5816
$Ba_{0.95}Ca_{0.05}Fe_{12}O_{19}$	20.82	12.00	3053	0.5763
$Ba_{0.9}Ca_{0.1}Fe_{12}O_{19}$	42.25	33.32	2184	0.7886
$Ba_{0.85}Ca_{0.15}Fe_{12}O_{19}$	65.05	34.11	1548	0.5244
$Ba_{0.8}Ca_{0.2}Fe_{12}O_{19}$	57.73	30.65	1621	0.5309

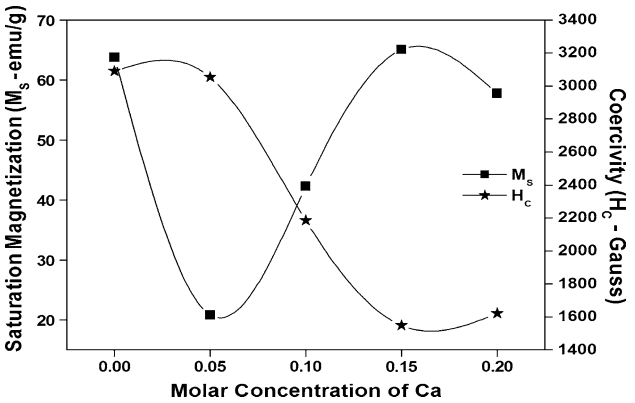

Fig. 6 Saturation magnetization versus coercivity for $Ba_{1-x}Ca_x$-$Fe_{12}O_{19}$ compounds

The variation in the magnetization nature of the present compounds may be explained on the basis of alternation in hyperfine fields and super exchange interactions. There are three factors for interpreting magnetization behaviour such as Fe^{3+}–O–Fe^{3+} super exchange interaction, spin canting (non-collinear magnetic order) and magnetic dilution. The initial decrease in saturation magnetization of calcium substituted compounds compared to the parent $BaFe_{12}O_{19}$ may be due to two effects such as magnetic dilution on 2a site and the spin canting promoted reduction of super exchange fields. The Fe^{3+}–O–Fe^{3+} super exchange interaction is disrupted and weakened by the substitution of Ca^{2+} ion and the canted spins result in lower magnetization. On the other hand, the magnetic collinearity breaks down after substitution of non-magnetic cation because of the disappearance of some super exchange interactions. In addition, spin canting or non-collinear magnetic order is a behaviour in which spin orientations of magnetic ions align in the preferred direction (c-axis for M structure ferrites) [27, 28]. While increasing the concentration of Ca, for $x = 0.15$ it is found that the saturation magnetization reaches the maximum value of 65.05 emu/g. The increase in saturation magnetization could be attributed to the enhancement of hyperfine fields at 12k and 2b sites as a result of Fe^{3+}–O–Fe^{3+} super exchange interaction [29].

The coercivity decreases from 3,090 Gauss to 1,548 Gauss for the Ca substitution of $x = 0$–0.15 whereas slight increase (1,621 Gauss) was observed for the compound with Ca concentration of $x = 0.2$. The decreasing trend in the coercive field (H_C) confirms the larger single domain particles present in the Ca substituted $BaFe_{12}O_{19}$ compounds. The slight increase in coercivity for $x = 0.2$ may be attributed to higher grain size with multi domain walls. This could be attributed to the microstructural defects which act as possible pinning centres for domain walls [30]. A large reduction in the coercivity value from 3,090 to 1,548 Gauss may be attributed to the fall in magneto crystalline anisotropy with respect to the amount of Ca^{2+} ion in the $BaFe_{12}O_{19}$ compounds [24].

The squareness ratio (M_R/M_S) for the pure and Ca substituted samples was found to be in the range of 0.5816–0.5244 except for the $Ba_{0.9}Ca_{0.1}Fe_{12}O_{19}$ compound whose M_R/M_S ratio was found to be 0.7886. The values close to 0.5 reveal that the compounds are formed with randomly oriented 3-D single domain particles with shape anisotropy. These results have good correlation with the morphology obtained from the scanning electron microscopic studies. At the same time, the $Ba_{0.9}Ca_{0.1}Fe_{12}O_{19}$ compound with the M_R/M_S ratio of 0.7886 partially shows 2-D behaviour possibly due to the powder form [31].

3.4.2 *High temperature magnetization studies*

The high temperature magnetic behaviour of $Ba_{1-x}Ca_x$-$Fe_{12}O_{19}$ compounds are recorded in the temperature range of 30 to 550 °C by using VSM with an applied field of 500

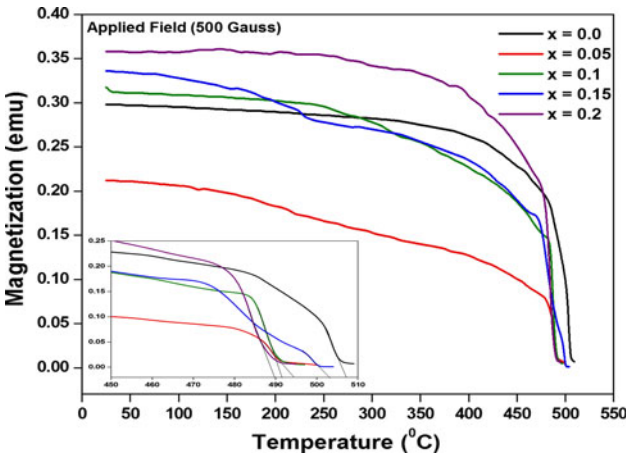

Fig. 7 Temperature dependent magnetization of $Ba_{1-x}Ca_xFe_{12}O_{19}$ compounds

Table 4 Curie temperature of the $Ba_{1-x}Ca_xFe_{12}O_{19}$ compounds

Sample details	Curie temperature (°C)
$BaFe_{12}O_{19}$	507.18
$Ba_{0.95}Ca_{0.05}Fe_{12}O_{19}$	494.47
$Ba_{0.9}Ca_{0.1}Fe_{12}O_{19}$	491.71
$Ba_{0.85}Ca_{0.15}Fe_{12}O_{19}$	503.13
$Ba_{0.8}Ca_{0.2}Fe_{12}O_{19}$	489.88

Gauss and the observed temperature dependent magnetization nature for these compounds are shown in Fig. 7. From the temperature dependent magnetization studies, it is observed that all the samples exhibit ferromagnetic to paramagnetic transition around 500 °C and the respective values are listed in Table 4. From the table, it is inferred that the Curie temperature is in decreasing trend upon increasing substitution level of Ca in the $BaFe_{12}O_{19}$ system. The improvement of saturation magnetization on increasing substitution of Ca is also identified with these studies. The room temperature and high temperature magnetization studies shows that the substitution of Ca in the Barium hexaferrite system diluted the magnetic property through sequential variation in saturation magnetization, remanent magnetization, coercivity and Curie temperature. The magnetically ordered BaFe particulate with higher saturation and low coercivity values shows the possibility for high-recording-density storage products [32].

3.5 Dielectric analysis

The dielectric studies are carried out to analyze the polarizability and to understand electron exchange between Fe^{2+} and Fe^{3+} while doping with Ca in the $BaFe_{12}O_{19}$ system. This study gives experimental values such as capacitance and dielectric loss for the frequency range between 50 Hz and 5 MHz at the room temperature. According to earlier reports, the dielectric polarization in ferrites is through a mechanism similar to the conduction process [17]. Since both the dielectric constant and electrical conductivity are basically electrical transport properties and their variation with temperature is similar, hence it may be assumed that the same mechanism is responsible for both the phenomenon [33–35]. The variation of dielectric constant with frequency for the pure and Ca substituted Barium Hexaferrite compounds are shown in Fig. 8.

Since all the compounds exhibit dominant electrode-sample polarization effect in the lower frequency region (<1 kHz), the dielectric analysis was carried out in the frequency region of 1,000 Hz–5 MHz. It is observed that the dielectric constant decreases rapidly with frequency in the low frequency region (<10 kHz) and reaches a constant

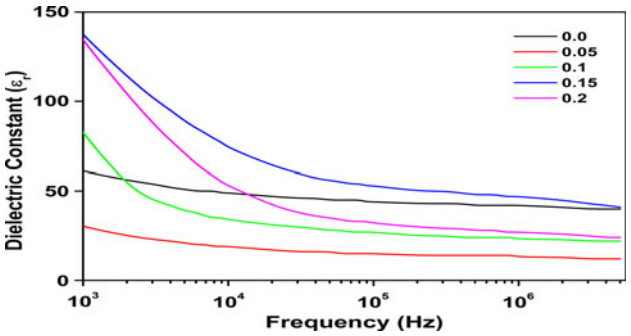

Fig. 8 Frequency dependent dielectric constant of $Ba_{1-x}Ca_xFe_{12}O_{19}$ compounds

value (limiting value) at high frequency region. The large value of dielectric constant in the lower frequency region is due to the interfacial polarisation at surfaces, dislocations pile ups of charges, oxygen vacancies and grain boundary defects [36]. In the present work, the rapid decrease in the dielectric constant at low frequency region may be attributed to Maxwell–Wagner type interfacial polarisation at the electrode-sample interface [37, 38]. It is also observed that, the dielectric constant values increases with increase in concentration Ca in the $BaFe_{12}O_{19}$ compounds except $Ba_{0.95}Ca_{0.05}Fe_{12}O_{19}$. This case may be explained on the basis of space charge polarization. The applied voltage on the sample drops mainly across the grain boundaries and a space charge polarization is built up at the grain boundaries. The space charge polarization is governed by the available free charges on the grain boundary and the conductivity of the sample. Koops proposed that the effect of grain boundaries is predominant at lower frequencies i.e. higher dielectric constant for thinner grain boundaries [39]. High dielectric constants show the decrease of penetration depth of the electromagnetic waves by increasing the skin effect. Hence, much lower dielectric constant values observed from the Ca substituted compounds at high frequencies warrant their importance in application point of view.

Dielectric loss factor is an important part of the total core loss in ferrites. Hence for low core loss, low dielectric losses are desirable. Dielectric loss factor tanδ represents the energy of dissipation in the dielectric system. The variation of tanδ as a function of frequency at room temperature is shown in Fig. 9. It is observed that for all the samples, the dielectric loss decreases continuously with increasing frequency. A maximum value of tanδ is observed when the jump frequency of electron between Fe^{2+} and Fe^{3+} is equal to the frequency of the applied field. The dielectric loss factor of the Ca substituted barium hexaferrites compounds decreases approximately inverse to the frequency. In the low frequency region which corresponds to high resistivity (due to grain boundaries and interfacial effects), more energy is required for electron exchange between Fe^{3+} and Fe^{2+} ions,

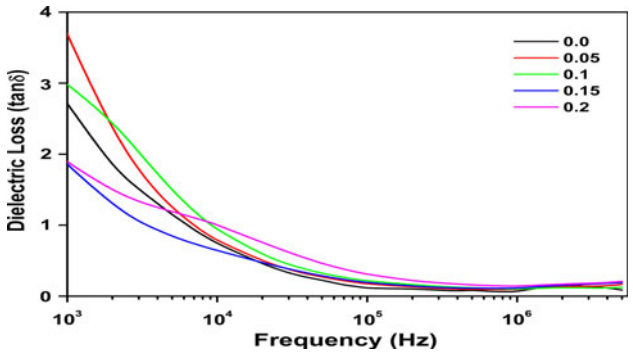

Fig. 9 Frequency dependent dielectric loss of $Ba_{1-x}Ca_xFe_{12}O_{19}$ compounds

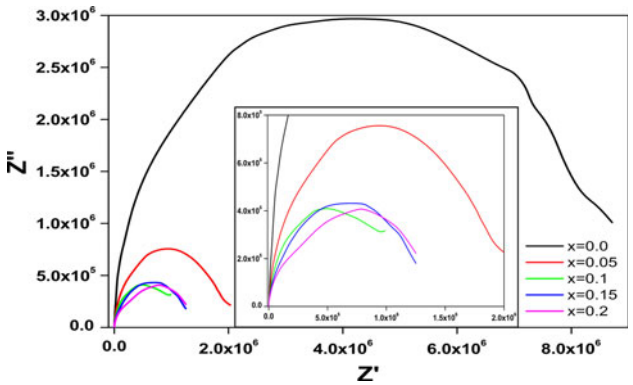

Fig. 10 Complex impedance plots of $Ba_{1-x}Ca_xFe_{12}O_{19}$ compounds

so that the energy loss is high. In the high-frequency range, which corresponds to low resistivity (due to grain), a small energy is needed for electron transfer between Fe^{3+} and Fe^{2+} in the grains and hence the energy loss is small [17].

Further, impedance properties of all the samples were studied as a function of frequency at room temperature in the range 50 Hz–5 MHz. The complex impedance data plots of all the samples shown in Fig. 10. In the figure, only single semicircle behavior was seen and it suggests that the contribution of electrical relaxation (dielectric relaxation) is mainly due to electronic charge carriers in single crystalline dielectric materials.

4 Conclusion

The Ca^{2+} substituted $Ba_{1-x}Ca_xFe_{12}O_{19}$ (where x = 0.05, 0.1, 0.15 and 0.2) compounds have been prepared through solid state reaction technique. The hexagonal magnetoplumbite crystal structure of all the prepared compounds was analyzed through powder X-ray diffraction analysis. From the scanning electron microscopic studies, it was observed that the morphology is uniform with flat hexagonal plates. The pure and Ca substituted $BaFe_{12}O_{19}$ compounds exhibit intense Raman resonance peaks which reveals the formation of well crystalline hexaferrite system. The variation in resonance peak positions observed in the frequency range below 150 cm^{-1} may be due to the effect of substitution of bivalent cations in $BaFe_{12}O_{19}$ system. The magnetization studies confirm the dilution of magnetic property while substituting Ca in the $BaFe_{12}O_{19}$ system and reveal the existence of spin canting effect which leads to the reduction of super exchange fields. A large reduction in the coercivity values in the Ca substituted $BaFe_{12}O_{19}$ compounds may be attributed to the fall in magneto crystalline anisotropy. The room temperature dielectric measurement suggests that the incorporation of Ca^{2+} in the $BaFe_{12}O_{19}$ system leads to the increase in dielectric constant and substantiates the space charge polarization.

References

1. L.L. Hench, J.K. West, *Principles of electronic ceramics* (Wiley-Interscience Publication, Singapore, 1990)
2. R. Nowosielski, R. Babilas, G. Dercz, L. Pajak Wrona, Structure and properties of barium ferrite powders prepared by milling and annealing. Arch. Mater. Sci. Eng. **28**, 735 (2007)
3. A.J. Moulson, J.M. Herbert, *Electroceramics*, 2nd edn. (Wiley, England, 2003)
4. Puneet. Sharma, R.A. Rocha, S.N. Medeiros, B. Hallouche, A. Jr Paesano, Structural and magnetic studies on mechanosynthesized $BaFe_{12-x}Mn_xO_{19}$. J. Magn. Magn. Mater. **316**, 29 (2007)
5. F.M.M. Pereira, C.A.R. Junior, M.R.P. Santos, R.S.T.M. Shon, F.N.A. Freie, J.M. Sasaki, J.A.C. de Paiva, A.S.B. Sombra, Structural and dielectric spectroscopy studies of the M-type barium strontium hexaferrite alloys ($Ba_xSr_{1-x}Fe_{12}O_{19}$). J. Mater. Sci. Mater. Electron. **19**, 627 (2008)
6. M.M. Rashad, I.A. Ibrahim, Improvement of the magnetic properties of barium hexaferrite nanopowders using modified co-precipitation method. J. Magn. Magn. Mater. **323**, 2158 (2011)
7. F. Kools, A. Morel, R. Grossinger, J.M. Le Bretond, P. Tenauda, LaCo-substituted ferrite magnets, a new class of high-grade ceramic magnets; intrinsic and microstructural aspects. J. Magn. Magn. Mater. **242–245**, 1270 (2002)
8. L. Lechevallier, J.M. LeBreton, J.F. Wang, I.R. Harris, Structural and mössbauer analyses of ultrafine $Sr_{1-x}La_xFe_{12-x}Zn_xO_{19}$ and $Sr_{1-x}La_xFe_{12-x}Co_xO_{19}$ hexagonal ferrites synthesized by chemical co-precipitation. J. Phys. Condens. Mater. **16**, 5359 (2004)
9. H. Yamamoto, M. Isono, T. Kobayashi, Magnetic properties of Ba–Nd–Co system M-type ferrite fine particles prepared by controlling the chemical coprecipitation method. J. Magn. Magn. Mater. **295**, 51 (2005)
10. P. Sharma, A. Verma, R.K. Sidhu, O.P. Pandey, Influence of Nd^{3+} and Sm^{3+} substitution on the magnetic properties of strontium ferrite sintered magnets. J. Alloys Compd. **361**, 257 (2003)
11. J.F. Wang, C.B. Ponton, R. Grossinger, I.R. Harris, A study of La-substituted strontium hexaferrite by hydrothermal synthesis. J. Alloys Compd. **369**, 170 (2004)
12. S. Kanagesan, S. Jesurani, R. Velmurugan, M. Sivakumar, C. Thirupathi, T. Kalaivani, Synthesis and magnetic properties of conventional and microwave calcined barium hexaferrite powder. J. Mater. Sci. Mater. Electron. **23**, 635 (2012)
13. S. Kanagesan, S. Jesurani, R. Velmurugan, S. Prabu, T. Kalaivani, Study of morphological and magnetic properties of

microwave sintered barium strontium hexaferrite. J. Mater. Sci. Mater. Electron. (2012). doi:10.1007/s10854-012-0620-1
14. S. Kanagesan, S. Jesurani, R. Velmurugan, S. Prabu, T. Kalaivani, Magnetic properties of Ni-Co doped barium strontium hexaferrite. J. Mater. Sci. Mater. Electron. (2012). doi:10.1007/s10854-012-0631-y
15. Yuping. Wang, Liangchao. Li, Hui. Liu, Haizhen. Qiu, X. Feng, Magnetic properties and microstructure of La-substituted BaCr-ferrite powders. Mater. Lett. **62**, 2060 (2008)
16. K.K. Mallick, P. Shepherd, R.J. Green, Magnetic properties of cobalt substituted M-type barium hexaferrite prepared by co-precipitation. J. Magn. Magn. Mater. **312**, 418 (2007)
17. M. Javed Iqbal, M. Naeem Ashiq, I. Hussain Gul, Physical, electrical and dielectric properties of Ca-substituted strontium hexaferrite ($SrFe_{12}O_{19}$) nanoparticles synthesized by co-precipitation method. J. Magn. Magn. Mater. **322**, 1720 (2010)
18. A. Ashima, S. Sanghi, A. Agarwal Reetu, Synthesis and characterization of $Ba_{1-x}Ca_xFe_{12}O_{19}$ hexaferrite synthesized by solid state reaction. AIP Conf. Proc. **1393**, 137 (2011)
19. C. Dong, PowderX: windows-95 based program for powder X-ray diffraction data processing. J. Appl. Crystallogr. **32**, 838 (1999)
20. Q. Fang, H. Cheng, K. Huang, J. Wang, R. Li, Y. Jiao, Doping effect on crystal structure and magnetic properties of chromium-substituted strontium hexaferrite nanoparticles. J. Magn. Magn. Mater. **294**, 281 (2005)
21. V. Berbenni, A. Marini, N.J. Welham, P. Galinetto, M.C. Mozzati, The effect of mechanical milling on the solid state reactions in the barium oxalate–iron(III) oxide system. J. Eur. Ceram. Soc. **23**, 179 (2003)
22. J. Kreisel, G. Lucazeau, H. Vincent, Raman spectra and vibrational analysis of $BaFe_{12}O_{19}$ hexagonal ferrite. J. Solid State Chem. **137**, 127 (1998)
23. J.M. Calderon Moreno, M. Yoshimura, Characterization by Raman spectroscopy of solid solutions in the yttria-rich side of the zirconia–yttria system. Solid State Ionics **154–155**, 125 (2002)
24. Gang. Xue, Cairong. Gong, Jinsheng. Liang, Guangchuan. Liang, Facile synthesis and characterization of $BaFe_{12}O_{19}$ nanoparticles with different morphologies. J. Dispers. Sci. Technol. **30**, 231 (2009)
25. Nobuyoshi. Koga, Takanori. Tsutaoka, Preparation of substituted barium ferrite $BaFe_{12-x}$ $(Ti_{0.5}Co_{0.5})_x$ O_{19} by citrate precursor method and compositional dependence of their magnetic properties. J. Magn. Magn. Mater. **313**, 168 (2007)
26. A.M.Y. El-Lawindy, S.A. Mansour, M. Hafiz, H.H. Hassan, A.A. Ali, Influence of the mole ratio, sintering condition and particle size on the magnetic properties of $BaFe_{12}O_{19}$ synthesized by ceramic method. Int. J. Appl. Ceram. Technol. **2**, 1 (2009)
27. H.C. Fang, C.K. Ong, X.Y. Zhang, Y. Li, X.Z. Wang, Z. Yang, Low temperature characterization of nano-sized $BaFe_{12-2x}Zn_xSn_xO_{19}$ particles. J. Magn. Magn. Mater. **191**, 277 (1999)
28. Suriya. Ounnunkad, Improving magnetic properties of barium hexaferrites by La or Pr substitution. Solid State Commun. **138**, 472 (2006)
29. Ugur. Topal, Husnu. Ozkan, Huseyin. Sozeri, Synthesis and characterization of nanocrystalline $BaFe_{12}O_{19}$ obtained at 850 °C by using ammonium nitrate melt. J. Magn. Magn. Mater. **284**, 416 (2004)
30. C. Doroftei, E. Rezlescu, P.D. Popa, N. Rezlescu, The influence of the technological factors on strontium hexaferrites with lanthanum substitution prepared by self-combustion method. J. Optoelectron. Adv. Mater. **8**, 1023 (2006)
31. Ugur. Topal, Factors influencing the remanent properties of hard magnetic barium ferrites: impurity phases and grain sizes. J. Magn. Magn. Mater. **320**, 331 (2008)
32. Takeshi. Harasawa, Ryota. Suzuki, Osamu. Shimizu, Sedat. Ölçer, Evangelos. Eleftheriou, Barium-ferrite particulate media for high-recording-density tape storage systems. IEEE Trans. Magn. **46**, 1894 (2010)
33. K. Iwauchi, Dielectric properties of fine particles of Fe_3O_4 and some ferrites. Jpn. J. Appl. Phys. **10**, 1520 (1971)
34. A.M. Shaikh, S.S. Bellad, B.K. Chougule, Temperature and frequency-dependent dielectric properties of Zn substituted Li-Mg ferrites. J. Magn. Magn. Mater. **195**, 384 (1999)
35. N. Rezlescu, E. Rezlescu, Dielectric properties of copper containing ferrites. Phys. Status Solid A **23**, 575 (1974)
36. J.C. Maxwell, *Electricity and magnetism*, vol. 1 (Oxford University Press, New York, 1973)
37. Yuanhua. Lin, Lei. Jiang, Rongjuan. Zhao, Ce.-Wen. Nan, High-permittivity core/shell structured NiO-based ceramics and their dielectric response mechanism. Phys. Rev. B **72**, 014103 (2005)
38. P. Kumar Jana, S. Sarkar, B.K. Chaudhuri, Maxwell-Wagner polarization mechanism in potassium and titanium doped nickel oxide showing giant dielectric permittivity. J. Phys. D Appl. Phys. **40**, 556 (2007)
39. C.G. Koops, On the dispersion of resistivity and dielectric constant of some semiconductors at audio frequencies. Phys. Rev. **83**, 121 (1951)